LBL-30299
Preprint

# Lawrence Berkeley Laboratory
UNIVERSITY OF CALIFORNIA

## Materials & Chemical Sciences Division

Submitted to Journal of the Electrochemical Society

# An in Situ Raman Spectroscopy Study of the Anodic Oxidation of Copper in Alkaline Media

S.T. Mayer and R.H. Muller

January 1991

| LOAN COPY |
|Circulates |
|for 4 weeks| Bldg. 50 Library.
LBL-30299
Copy 2

Prepared for the U.S. Department of Energy under Contract Number DE-AC03-76SF00098.

## DISCLAIMER

This document was prepared as an account of work sponsored by the United States Government. While this document is believed to contain correct information, neither the United States Government nor any agency thereof, nor the Regents of the University of California, nor any of their employees, makes any warranty, express or implied, or assumes any legal responsibility for the accuracy, completeness, or usefulness of any information, apparatus, product, or process disclosed, or represents that its use would not infringe privately owned rights. Reference herein to any specific commercial product, process, or service by its trade name, trademark, manufacturer, or otherwise, does not necessarily constitute or imply its endorsement, recommendation, or favoring by the United States Government or any agency thereof, or the Regents of the University of California. The views and opinions of authors expressed herein do not necessarily state or reflect those of the United States Government or any agency thereof or the Regents of the University of California.

LBL-30299

# AN *IN SITU* RAMAN SPECTROSCOPY STUDY OF THE ANODIC OXIDATION OF COPPER IN ALKALINE MEDIA

Steven T. Mayer* and Rolf H. Muller

Materials Sciences Division
Lawrence Berkeley Laboratory

and

Department of Chemical Engineering
University of California
Berkeley, California 94720

## Abstract

*In situ* Raman spectroscopy measurements were made during the anodic oxidation of copper in 1M and 6M KOH solutions. The formation of $Cu_2O$ occurs at potentials corresponding to the first anodic voltammetric peak (A1), and a porous layer of $Cu(OH)_2$ composed of fine needle-like crystals is formed at the second voltammetric peak (A2). The compact underlayer of cuprous oxide is transformed to another species (presumably CuO) at potential above 0 mV vs. Hg/HgO. At potentials near oxygen evolution, an unidentified trivalent species appears. The reduction of the oxide is shown to be strongly influenced by illumination. Under irradiation, the underlayer is first reduced to $Cu_2O$ at around 0 mV vs. Hg/HgO, followed by $Cu(OH)_2$ reduction to copper, and finally $Cu_2O$ reduction to copper metal. Without intense illumination, the p-type semiconductive properties of the underlying $Cu_2O$ layer acts as a Schottky barrier, causing the large degree of irreversibility found in this system.

*Present address: Lawrence Livermore National Laboratory, Livermore, CA 94550

---

This work was supported by the Assistant Secretary for Conservation and Renewable Energy, Deputy Assistant Secretary for Utility Technologies, Office of Energy Management, Advanced Utility Concepts Division of the U.S. Department of Energy under Contract No. DE-AC03-76SF00098.

## Introduction

Most of the present understanding of electrochemically formed anodic films has been derived from electrochemical measurements. Additional information on the physical and chemical structure of the films can be determined by use of in situ optical techniques. Raman spectroscopy was used here for identifying surface species and investigating the photo-induced transformations of films. In the present study, laser Raman spectroscopy, in conjunction with electrochemical measurements, was used to explore the physical and chemical nature of anodic films on copper in 1M and 6 M KOH.

There are three copper oxide and hydroxide compounds which are known to be stable as bulk solids at ambient temperatures. These are $Cu_2O$ (cuprous oxide), CuO (cupric oxide) and $Cu(OH)_2$ (cupric hydroxide). All three of these materials have been suggested as being present in various forms on copper electrode surfaces in alkaline media [1,2].

Thermodynamic calculations indicate that at least one monovalent and two divalent soluble copper species are expected to be formed in alkaline electrolytes. Cuprous oxide has a very low solubility, but the cuprous ion has been detected using a ring/disk apparatus [3]. The solubility of this ion is expected to increase with increasing pH. Cuprous oxide can react with water or hydroxide ion to form a cupric ion. Various divalent copper species are believed to exist, but only the blue cuprite ($CuO_2^{-2}$) and bicuprite ($HCuO_2^{-1}$) ions predominate at high pH. Solid $Cu(OH)_2$ is considerably more soluble than CuO at pH 14 ($2.1 \times 10^{-3}$ vs $1.1 \times 10^{-5}$M), though CuO is thermodynamically more stable. Figure 1 shows the reversible potentials of various reactions of copper in 1M KOH vs. the Hg/HgO (in 1M KOH) reference electrode derived from the data presented in the literature [1,2,4].

The existence of other copper oxide or hydroxide films has been suggested. Droog et. al. [5,6] have studied the adsorption of oxygen on copper using voltammetry and ellipsometry. They detected the reversible formation of a submonolayer film at potentials

cathodic of bulk $Cu_2O$ formation, which may be associated with the formation of an underpotential oxide or hydroxide (CuOH). Muller [7] was perhaps the first to propose that a trivalent copper oxide species exists on the electrode surface near the potential of oxygen evolution. He stated that the surface oxide turned an orange-yellow color at highly anodic potentials. The results of Miller [3], using a ring disk apparatus, indicated that a species of higher valency (i.e. greater than 2) is reduced at around 0.5 V vs SCE. This oxide might be unstable $Cu_2O_3$.

The mechanism of cuprous oxide film formation is still controversial. The structure has been described as 1) porous [8-10], 2) growing two- or three- dimensional crystals [11,12], compact and homogeneous [13] and 3) a compact underlayer with a precipitated upper layer [14]. These structures imply two possible mechanism for cuprous oxide film formation, 1) a solid-state mechanism, presumably with oxygen ion diffusion into the copper lattice [13, 15, 16] and 2) and a dissolution/precipitation mechanism [8, 12, 17]. The low solubility of cuprous oxide does not necessarily rule out the dissolution/precipitation mechanism, and since the cuprous ion becomes more soluble with increasing pH, this mechanism might dominate at higher pH.

Miller [3] has shown that there is a considerable potential range for active copper dissolution to form $Cu^{+2}$ species. This implies that there is a considerable range of potentials over which cuprous oxide or copper can react to form cupric ion at a concentration below that of the solubility limit of the ion. Several reaction mechanisms have been presented to account for a dissolution process occuring either from copper or from cuprous oxide [4, 9, 10, 18]. Based on the relative charge passed in the monovalent versus the divalent voltammetry peaks, a simple consecutive oxidation of Cu to $Cu_2O$ followed by $Cu_2O$ to CuO or $Cu(OH)_2$ has been rejected [18]. Clearly, solution-side processes are quite important at higher pH.

The mechanism for the electrochemical reduction of surface oxides to copper metal is not well understood. There is a large degree of irreversibility in the reduction of the

surface material [17]. Pyun [19] has reported that the anodic surface layers can only be completely reduced after a long time and at very cathodic potentials. The reported large difference in the potentials of oxidation and reduction demonstrates this point.

An in situ Raman spectroscopy study of the electrochemical oxidation of Cu in 0.1M NaOH has previously been reported [17]. The investigators used cyclic and potential step voltammetry. They reported that $Cu_2O$ was detected at 400 mV anodic of the normally associated voltammetric peak. $Cu_2O$ continued to be detected up to a potential 1 volt anodic of the monovalent oxidation peak. Near the potential where oxygen evolves, scattering from $Cu_2O$ was reported to diminish and an (unidentified) broad band was observed. It was suggested that this band was due to the "overlap of hydroxide and cuprous oxide spectra", or the "formation of a polymeric species of the form $(Cu_n(OH)_{2n-2})^{2n}$". The broad band disappears and scattering from cuprous oxide reappears during the cathodic potential sweep. Discrepancies between voltammetric and spectroscopic observations were attributed to nucleation and kinetic effects.

Raman spectroscopy is used along with voltammetry to help solve some of the unanswered questions concerning the copper system in alkaline media. Solutions of higher alkalinity than those discussed above were studied so as to be able to determine the effect of changes in solubility on the film formation process. The objectives of this study were to investigate 1) the formation and transformation of the anodic copper film in 1 and 6M KOH, 2) illumination effects on these processes, and 3) the reason for differences between voltammetric and spectroscopic results.

## Apparatus and Proceedures

The apparatus used in this study has been discussed in detail elsewhere [20]. An argon ion laser tuned to 488 nm (peak output power 100 mW) was focused to a 45 um spot on the surface resulting in an irradience of approximately $1.5 \times 10^3$ W/cm$^2$. Prior to striking the surface, the beam passes through a sharp band pass filter centered at 488 nm (10 nm FWHM), effectively removing all plasma lines from the incident beam.

The electrochemical cell used the optimal angles of incidence (70$^o$ from the surface normal) and collection (60$^o$ from the surface normal in the plane perpendicular to the plane of incidence) of Raman scattered light from thin films as derived theoretically [21-23] and verified experimentally [24]. The cell was made of Teflon and contained ports for the introduction and removal of deoxygenated electrolyte. A Pt screen counter electrode and a Hg/HgO reference electrode were used, both of which fit into the same chamber as the mechanically polished and cleaned copper working electrode (see below).

The scattered light from the surface is focused on the entrance slit of a single monochromator using a 5 cm f/1.4 lens placed 2 inches from the illuminated spot. Rayleigh scattered light is separated from the light entering the monochromator by placing sharp band pass filters (Omega Co.) in the beams path. These filters allow only 1 part in a million of the Rayleigh scattered light to pass and have an 80% transmission at 200 cm$^{-1}$. The use of these filters with a single monochromator results in a significant improvement in the collection efficiency over conventional double and triple monochromators. A 1024 channel intensified photodiode array was used as a detector and the data were processed by an EG&G Par OMA III system.

Cu (111) crystals (99.999%) were imbeded in an epoxy mold. The surfaces were polished using a series of diamond paste polishing compounds of decreasing size (down to 0.25 um). A final polish with a colloidal silica suspension (0.05 um) created a fine mirror finish. The electrodes were then rinsed in a series of organic solvents of increasing

polarities, and finally in distilled water. The optical constants of these surfaces as obtained by spectroscopic ellipsometry were consistent with those reported in the literature [20].

After placing the electrode in the cell, the potentiostat was turned on and the electrode potential set to -700 or -600 mV vs. a Hg/HgO reference electrode. Next, the cell was filled with a deoxygenated 1 or 6M KOH solution. Ellipsometry result have shown that a thin cuprous oxide film can form (even in deoxygenated electrolyte) within 1-2 min. if this cathodic protection was not applied.

## REFERENCE SPECTRA

Reference spectra for $Cu_2O$, $Cu(OH)_2$, and CuO have been reported by Hamilton et al [17]. Shown in Figure 2 are Raman spectra of compressed powder pellets of $Cu_2O$, CuO and $Cu(OH)_2$. These results are in agreement with those previously reported. The optical spectra of $Cu_2O$ exhibit an interband transition near 2.1 eV [25], as well as some fine structure near this energy due to exciton electron-hole pairing. The proximity of this interband transition to the excitation wavelength used in this study (i.e. the 488 nm line of the $Ar^+$ ion laser), as well as the relative stability of excitons, resulted in some resonance enhancement. $Cu(OH)_2$ has an absorption edge in the visible region, and this may cause it to also exhibit resonance Raman enhancement. The large cross section for scattering from $Cu_2O$ and $Cu(OH)_2$ make their detection relatively easy. The assignment of these peak to their associated phonons is presented elsewhere [20]. CuO is a much weaker scatterer than either $Cu_2O$ or $Cu(OH)_2$. Also, the major Raman band of CuO coincides with that of $Cu_2O$ (at around 633 nm). Therefore, CuO is very difficult to detect using this technique.

We found that our $Cu_2O$ powder standard did not decompose under intense illumination. Hamilton et. al. [17] reported that it was necessary to reduce their laser power below 60 mW in order to observe a $Cu(OH)_2$ spectrum (an energy density was not given), and suggested that at higher powers $Cu(OH)_2$ thermally decomposed in air to CuO and water. Our findings support this idea. Figure 3 shows the time dependence of the 488 $cm^{-1}$ $Cu(OH)_2$ peak of a compressed powder in air (90 mW total power, energy density $1.4 \times 10^3$ $W/cm^2$). The Raman scattering intensity decreases to half of its initial value within 100 seconds. This result demonstrates the possibility of a thermal conversion process hampering the interpretation of our in situ spectra. We therefore also obtained time-dependent spectra from the $Cu(OH)_2$ compressed powder pellet in a 1M KOH solution (Figure 4A). When immersed in the aqueous solution, the rate of change of the peak intensity was considerably smaller (only 2% per 100 seconds), indicating that thermal

decomposition would not be as great an issue for in situ studies. However, since integration times of up to 100 seconds were necessary in some of our experiments, even a small decrease of 2% might cause a misinterpretation of the results. We reasoned that electrochemically formed $Cu(OH)_2$ would be in close proximity to an excellent heat conductor (i.e. the copper electrode), and the rate of thermal decomposition might be reduced further. The time dependent intensity of the 488 $cm^{-1}$ Raman peak of an electrochemically formed $Cu(OH)_2$ film (taken in air) is shown in Figure 4B. We note that the intensity is invariant with time and that the presence of the metal electrode alone should be sufficient to diminish the photothermal dehydration of the hydroxide.

## Potential Sweeping Experiments

Potential sweep experiments were performed in both 1M and 6 M KOH at 1/2, 1, and 10 mV/sec. As described above, the sweeps were begun at a potential cathodic of all copper oxidation reactions. Raman data shown are background corrected for all signals not associated with film formation. Some sources of this background signal include 1) dark current noise (thermal noise associated with the intensified diode array detector), 2) readout noise (related to digitalization of the data), 3) Rayleigh scattering "leakage" photons which scatter inside the monochromator, and 4) background Raman scattering from the electrolyte [20].

A 10 mV/sec voltammogram of Cu in 1M KOH is shown in Figure 5, and illustrates the major anodic and cathodic peaks for the system. The first anodic peak (referred to as the the A1 peak) is located at -400 mV vs. Hg/HgO and is generally associated with a monovalent oxidation process. The second anodic peak (A2), at around -25 mV, may actually be two separate overlapping peaks, since it has a shoulder near -150 mV. Very little current is passed beyond the A2 peak up to 600 mV, where the onset of oxygen evolution begins. On the reverse sweep, the small (C2) peak is seen at -475 mV. The (C1) peak becomes complex at higher pH, having a shoulder at -800 mV, and a maximum at -1000 mV vs. Hg/HgO.

## Anodic Potential Sweep

Raman spectra obtained during a 1 mV/sec potential sweep in 1 and 6 M KOH are shown in Figures 6 to 8. The spectra are offset to improve their readability. Raman spectra were collected for 100 second, and therefore spectra shown are averaged over a 100 mV potential range. The current and integrated intensities of the bands associated with $Cu_2O$ and $Cu(OH)_2$ are plotted as a function of potential in Figures 9 and 10. The intensities are arbitrarily given negative values during the cathodic sweep so as to make the figures more readable. For potentials cathodic of the A1 peak, the spectra are similar to that of a KOH solution and change little up to -350 mV (this background spectrum from the electrolyte is subtracted from all spectra shown). At a potential of around -375 mV, a Raman band at 635 $cm^{-1}$ is seen, indicating the formation of a $Cu_2O$ film (Figure 6A). Note that this potential corresponds to that of the location of the A1 peak and that this observation is in contrast to the results of Hamilton et. al. [17], who showed (at pH 13) that a $Cu_2O$ film was not observed until 300 mV anodic of the first oxidation peak. (Our results show that in general, at higher sweep rates and lower pH the appearance of the $Cu_2O$ signal is delayed). Increases in the potential up to 50 mV in 1M KOH and 400 mV in 6 M KOH result in an increase in the intensity of the $Cu_2O$. Coinciding with the second anodic voltammetry peak at around -100 mV, the formation of a $Cu(OH)_2$ film is identified by a band at 488 $cm^{-1}$. The level of "white" background scattering also increases near this voltage*. The size of the $Cu(OH)_2$ Raman peak does not change significantly above -50 mV, but the $Cu_2O$ band diminishes at higher potentials.

Figure 7 compares the Raman spectra taken at 450 and 650 mV in 1M KOH. At the latter potential, oxygen evolution begins and a broad Raman band centered at around 550 $cm^{-1}$ and 300 $cm^{-1}$ in width is observed together with the 488 $cm^{-1}$ band. The $Cu_2O$ band

---

* This phenomenon is possibly associated with a breakdown of phonon scattering selection rules for small $Cu(OH)_2$ crystals.

is not seen. The location and breadth of this band is similar to the band which Hamilton et. al [17] attributed to $Cu(OH)_2$ scattering.

The fact that we observe the same broad band peak at the same potential as Hamilton et. al. (in addition to a cupric hydroxide peak) strongly indicates that the species which it represents is not the hydroxide but rather some new compound. This finding could indicate the presence of a trivalent oxide of copper, perhaps $Cu_2O_3$, in agreement with Miller's ring/disk measurements [3].

Several conclusions can be drawn from the results shown in Figures 6 to 10. Cuprous oxide forms at a potential near that of the observed A1 current peak; cupric hydroxide is formed at potentials near the A2 peak. In contrast to the results at lower pH, the rate of $Cu_2O$ film formation has increased dramatically upon increasing the hydroxide concentration by a factor of 10. In 6M KOH, $Cu_2O$ formation coincides with the A1 voltammetry peak and the scattering from the film is quite strong, indicating it is considerably thicker at higher pH (see below).

The formation of a cupric hydroxide film is clearly supported by our data (again, in contrast with the results of Hamilton et al. [17] at pH 13). Increases in pH increase the $Cu(OH)_2$ scattering signal, indicating that the formation of this film is enhanced by the presence of hydroxide ion. This finding might have been expected since the balanced reaction of cuprous oxide to form cupric hydroxide involves the hydroxide ion as a reactant. Any addition of this ion would be expected to drive the reaction toward the cupric hydroxide product (Le Chatelier's Principle).

Our data show that at potentials near the A2 voltammetry peak, both $Cu_2O$ and $Cu(OH)_2$ are present at the electrode surface, but the distribution of the compounds (within the film) is unknown. If the materials are dispersed evenly, a linear relation between the amount of material and the band intensity should be valid. On the other hand, if the film has a laminated structure (one film on top of the other), the penetration of light to and from the underlayer will be diminished by the presence of the overlayer. Since cuprous oxide is

the sole reaction production at lower potentials, we might suppose that it is still present at the metal/film interface at higher potentials. The buildup of divalent soluble species will eventually supersaturate the interfacial region, resulting in hydroxide precipitation. The growth of this film could lead to a diminished level of scattering from the underlayer of cuprous oxide due to a limited light penetration depth. SEM photographs of the hydroxide film (Figure 11) show the hydroxide film is composed of fine, needle-like crystals. These crystals should scatter light (as seen by our elastic light scattering measurement of the system [20]), and may diminish the Raman signal from a cuprous oxide underlayer.

However, for this hypothesis to be true, the hydroxide peak should increase in size while the cuprous oxide peak decreases, a result not observed. Furthermore, since little or no charge is passed at potentials anodic of the A2 voltammetry peak (where the cuprous oxide band is seen to decrease in size), we suggest that $Cu_2O$ may be transformed to CuO via a photochemical solid state process, as will be explained elsewhere [26].

All our result show that the intensity of the $Cu_2O$ band decreases at potentials anodic of the A2 voltammetry peak. In our 1 mV/sec, 1M KOH experiment the Raman signal completely disappears from the spectra at potentials anodic of 550 mV. A similar experiment run at 10 mV/second shows this band decreasing to only half its maximum value at the same potential. When the time for the process to occur is considered, the average rate of film transformation is seen to be only about five times faster at the higher sweep rate. It is reasonable to assume that the thickness of the cuprous oxide film formed at the higher sweep rate will be, at most, equal to that formed at the slower sweep rate. Therefore, this result implies some degree of diffusion limitation for this reaction.

To help differentiate between the time versus potential dependence of the monovalent/divalent transformation process, another 10 mV/second potential sweep experiment was performed in which the potential was held at the maximum anodic value (600 mV) for 100 seconds before reversing the direction of the sweep (Figure 12). Comparison of the two 10 mV/sec experiments show them to be similar up to the constant

potential point of the experiment. The $Cu_2O$ signal continues to decrease during the constant potential period for another 40 second before the film is completely transformed.

## REDUCTION OF COPPER FILMS

Raman spectra obtained during the cathodic scan of 1 and 6 KOH, 1 mV/second experiments are shown in Figure 6B, Figure 8B and Figure 8C. The broad band at 550 $cm^{-1}$ completely disappears at a potential of 450 mV, though the cupric hydroxide peak size is unaltered. Further deceases in potential result in an increase (in 6M KOH) or a reappearance (in 1M KOH) of the $Cu_2O$ band intensity. The hydroxide is reduced first, followed by the reduction of the (reformed) $Cu_2O$. The reappearance and/or dramatic increase in the $Cu_2O$ signal on the cathodic sweep is observed though the size of the hydroxide peak is virtually unchanged over the potential range of 0.6V to -0.5V. Both the cuprous oxide and cupric hydroxide are reduce prior to the major cathodic peak seen in the voltammetry.

In the 10 mV/second/potential arrest experiment (Figure 12) the intensity of the cuprous oxide peak is almost twice that observed on the anodic sweep. This finding is most likely due to a continued thickening of an underlying CuO film during the potentiostatic phase, which is subsequently reduced to $Cu_2O$. We rule out a mechanism to explain these observations in which the cupric hydroxide film is reduced to form cuprous oxide because 1) the intensity of the cuprous oxide band increase with potential arrest time during the cathodic sweep and 2) the intensity of the hydroxide band does not significantly change during the arrest time. All of the results above taken together point to the fact that, while the most important parameter for cuprous oxide film transformation to CuO is the potential, some solid-state diffusion/migration controlled process on the time scale of 10-100 seconds is also involved.

## Effects of Illumination on $Cu_2O$ Reduction

The reduction of the oxides during the cathodic sweep is complex. The cuprous oxide reduction potential under illumination becomes increasingly more anodic as the sweep rate is decreased. The role of the $Cu_2O$ layer in the film formation and reduction process is unclear. The reappearance of $Cu_2O$ during the cathodic sweep is unexpected since it is accompanied by no cathodic charge and occurs at a potential anodic of the reversible potential (see Figure 1). Because only a small part of the electrode surface is illuminated by the laser, some experiments were performed to determine if the behavior of the illuminated area might be different from that not illuminated.

Data obtained during a 1 mV/second potential sweep in 1M KOH with a maximum anodic potential of -200 mV (i.e. at a potential just before the onset of the divalent process) do not indicate the presence of $Cu(OH)_2$. Under these conditions the $Cu_2O$ film formed during the anodic sweep is reduced at -450 mV, indicating an almost reversible process under illumination. In contrast to this, the peak of the voltammetric reduction wave is located around -600 mV for this experiment.

All of the data discussed so far points to the difference between the film formation and reduction processes under illumination (as determined by our Raman spectra) versus those in the dark (illustrated by the voltammetry). Figure 13 helps to clarify the discrepancy between the two conditions by showing two potential sweep experiments, with $Cu_2O$ peak intensity, potential, and current all plotted with respect to time. Both experiments involve an anodic sweep to -300 mV in which a cuprous oxide film is formed. Also, both have a 10 minute potential arrest during the cathodic sweep, either at -500 or -600 mV. During this arrest period, the spot of illumination on the sample is moved by moving the cell with a micrometer. In this fashion, a previously unilluminated portion of the surface is probed. In Figure 13a, (potential arrest at -500 mV), after moving the cell there is a large increase in the Raman signal, which falls off rapidly. However, Figure

13b ( potential arrest at -600mV) shows that, after moving the cell, no increase in signal is seen. We can conclude from Figure 13 that the (dark) $Cu_2O$ film is reduced somewhere between -500 and -600 mV under these conditions. This finding is consistent with the voltammetry shown in Figure 13. In the one case a reduction wave has already occured prior to moving the cell, whereas it hasn't in the other. In both cases the peak potential of the reduction wave is around -550 mV.

## Potential Step Experiments

The intensity of the 633 $cm^{-1}$ cuprous oxide band versus the square root of time following the application of a potential step from -600 to potentials between -250 to -350 mV is linear [20], in agreement with the result of Hamilton et. al. [17]. Assuming that the integrated intensity is proportional to the film thickness, this parabolic dependence indicates a diffusion-controlled growth of the oxide layer [27,28], and is consistent with ellipsometry results [20].

A more complicated behavior is observed when the potential is stepped to a value where divalent species are formed. The current transient following the application of a potential step from -600 to -150 mV is shown in Figure 14A. The very large initial current density (upwards of 25 $mA/cm^2$ ) decreases rapidly to values on the order of 0.2 $mA/cm^2$ within 200 seconds. Afterwards, the current decreases slowly. The associated Raman spectra as a function of time are shown in Figure 14B. Quite quickly (within 50 seconds) the cupric hydroxide band is seen with a very small cuprous oxide band. Later, the intensity of both peaks increases, with the intensity of the cuprous oxide band becoming larger at later times. The integrated intensity of these bands is shown in Figure 15. The intensity of both bands increases in an approximately linear manner. (The apparent decrease in the intensity of the hydroxide peak in the second spectrum is actually a decrease in the background scattering level, attributed to the formation of small crystals.)

Since the intercept of the hydroxide peak is significant, it appears that hydroxide film growth occurs rapidly during an initial period (under 50 seconds). Later, the hydroxide peak intensity grows more slowly (increasing only about 50% in 30 minutes). Extrapolation of the cuprous oxide intensity to zero time indicates a near zero intensity intercept.

Since cuprous oxide is not initially present, the large initial current is associated with the formation of the hydroxide and soluble divalent copper on an almost cuprous oxide free surface. The linear growth of the cuprous oxide layer at high potentials is consistent with our elastic scattering measurements [20], which showed that the oxide was dissolving to form the soluble divalent species. The growth of this now porous layer is controlled by the rate of hydroxide reaction with the metal (kinetic controlled/linear growth) and not the diffusion of oxygen, hydroxide, or metal ions in a compact underlayer (parabolic/diffusion controlled growth). The growth of the hydroxide is controlled by the availability of divalent species formed at the surface, which in turn is controlled by the competing rate of cuprous oxide formation and dissolution.

## Conclusions

Reference spectrum of CuO, $Cu_2O$, and $Cu(OH)_2$ are in agreement with those previously reported. We have demonstrated that these materials are either stable under laser illumination (CuO and $Cu_2O$) or that the thermal decompositon of the film is negligible in the presence of an aqueous solution and a metal electrode ($Cu(OH)_2$). The transformation of the oxide layers on copper is influenced by illumination and is an electrochemical rather than thermal process.

At sufficiently slow sweep rates, the formation of cuprous oxide is observed at potentials coincident with the monovalent voltammetric oxidation peak. At higher sweep

rate the appearance of the cuprous oxide band is slightly delayed. There appears to be a concurrent dissolution process that contributed to the voltammetric current and occurs along with cuprous oxide film formation.

$Cu(OH)_2$, rather than the thermodynamically preferred CuO, forms at potentials coincident with the voltammetric divalent oxidation peak (A2). This finding should be contrasted with the results of Hamilton et. al. [17], who did not observe the species at pH 13. The kinetics of hydroxide formation is favored at higher pH.

Potential-step/Raman measurements show that at moderate potentials cuprous oxide film growth is parabolic, indicative of a diffusion controlled process. For higher potential steps, the film growth is linear. Under these conditions, cupric hydroxide initially forms very rapidly on a cuprous-oxide-free surface, and is correlated with the initially high current density. Later, the rate of cupric hydroxide growth is greatly diminished as the cuprous oxide layer is formed. The appearance of the cuprous oxide layer decreases the rate of divalent copper formation.

At potentials above the A2 peak, the compact underlayer of cuprous oxide is transformed to CuO. The thermodynamic potential for this reaction is shifted anodically under illumination since CuO is reduced to cuprous oxide at potentials 300 mV anodic of the dark divalent formation reaction.

A broad band observed at 550 $cm^{-1}$ and found near oxygen evolution potentials was previously interpreted as being due to the presence of a hydrated or polymeric form of cupric hydroxide. We believe that the appearance of this band is due to the formation of a trivalent copper surface species (possibly $Cu_2O_3$ ) via a solid-state transformation of CuO.

Reduction of cuprous oxide to copper metal is strongly influenced by illumination. The reduction potential of the oxide under illumination can approach that of the thermodynamic potential under certain conditions. In the dark, the reduction occurs with a large overpotentials. The p-type semiconductive oxide appears to act as a Schottky barrier (i.e., like a diode). Illumination generates charge carriers which minimize the resistance of

the layer and allow for its reduction at a more reversible potential. The effectiveness of this barrier layer decreases with increasing pH. It is the presence of the cuprous oxide layer which is responsible for the large degree of irreversibility of the system.

This work was supported by the Assistant Secretary for Conservation and Renewable Energy, Deputy Assistant Secretary for Utility Technologies, Office of Energy Management, Advanced Utility Concepts Division of the U.S. Department of Energy under Contract No. DE-AC03-76SF00098.

## References

1. Bertocci, U., and Donald D. Wagman, Standard Potentials in Aqueous Solutions, Allen J. Bard, Roger Parsons, and Joseph Jordan, Editors. Marcel Dekker, New York, 1985.

2. Bertocci, U., and Dennis R. Turner, Encylopedia of Electrochemistry of the Elements, Vol. II, Allen J. Bard, editor. Marcel Dekker, New York, 1974.

3. Miller, B., This Journal , **116**, 1675 (1969)

4. De Zoubov, N., C. Vanleugenhaghe, and M. Pourbaix, Atlas of Electrochemical Equilibria in Aqueous Solutions, Sect. 14.1, Marcel Pourbaix, editor. Pergamon Press, New York, 1966.

5. Droog, J. M. M., C. A. Alderliesten, P. T. Alderliesten, and Gosse A. Bootsma, J. Electroanal. Chem. **111**, 61 (1980).

6. Droog, J. M. M., and B. Schlenter, J. Electroanal. Chem. **112**, 387 (1980).

7. Muller, E., Z. Elektrochem. **13**, 133 (1907).

8. Yamashita, M. K. Omura, and D. Hirayama, Surf. Sci. **96**, 443 (1980).

9. Shoesmith, D. W., T. E. Rummery, D. Owen, and W. Lee, This Journal , **122**, 651 (1974)

10. Shoesmith, D. W., S. Sunder, M. G. Bailey, G. J. Wallace, and F. W. Stanchel, J. Electroanal. Chem. **143**, 154 (1983).

11. Fletcher, S., R. G. Barradas, and J. D. Porter, This Journal, **125**, 1960 (1978).

12. Ashworth, V. , and D. Fairhurst, This Journal, **124**, 506 (1977).

13. Strehblow, H. H., and B. Titze, Electrochim. Acta **25**, 839 (1980).

14. Ord, J. L., D. J. DeSmet, and Z. Q. Huang, This Journal , **134**, 826 (1987).

15. Hampson, N. H., J. B. Lee, and K. I. MacDonald, J. Electroanal. Chem. **32**, 165 (1971).

16. Shoesmith, D. W., W. Lee, and M. G. Bailey, Electrocrystallization, R. Weil and R. G. Barradas, editors. Electrochemical Societry Softbound Proceedings Series, Pennington, NJ, 1981.

17. Hamilton, J. C., J. C. Farmer, and R. J. Anderson, This Journal, **133**, 739 (1986).

18. Macdonald, D. D., ibid., **122**, 651 (1974).

19. Pyun, Chong-Hong, and Su-Moon Park, ibid., **133**, 2024 (1986).

20. Mayer, Steven T., Ph. D. Thesis, University of California at Berkeley, Dept. of Chem. Eng., December, 1989. Lawerence Berkeley Laboratory Report LBL-15607.

21. Greenler, Rober G., and T. L. Slaner, Spectrochim. Acta **29A**, 193 (1973).

22. Dilella, D. P., A. Gohin, R. H. Lipson, P. McBreen, and M. Moskovits, J. Chem. Phys. **73**, 4282 (1980).

23. Ager, J. W., D.K. Veirs, and G. M. Rosenblatt, J. Chem. Phys., **92**, 2067, 1990.

24. Mullins, David R., and Alan Campion, J. Phy. Chem. **88**, 8 (1984).

25. Landolt and Bornstein, Numerical Data and Functional Relationships in Science and Technology, New Series, Group III: Crystals and Solid State Physics. Volume 17, Semiconductors, Subvolume 4. Physics of Non Tetrahedrally Bonded Elements and Binary CompoundsI. O. Madelung, Editor. Berlin, 1983.

27. D. T. Schwartz and R. H. Muller, submitted to Surf. Sci.

27. Dibenedetto, A. T., The Structure and Properties of Materials, McGraw-Hill, 1967.

28. Fromhold, A. T., Jr., Theory of Metal Oxidation: Volume 1 and 2. Elsevier North-Holland, New York, 1976.

## Figure Captions

1) Thermodynamic potentials of various reactions of copper in 1M KOH versus the Hg/HgO (in 1M KOH) reference electrode.

2) Raman spectra of compounds investigated: top- $Cu_2O$ compressed powder, 40 mW laser power, 5 min. exposure; middle- $Cu(OH)_2$ compressed powder, 40 mW laser power, 5 min. exposure; bottom- CuO compressed powder, 90 mW laser power, 45 min. exposure.

3) Integrated intensity of the 488 $cm^{-1}$ peak of $Cu(OH)_2$ powder in air as a function of time. Laser power 90 mW.

4) Integrated intensity of the 488 $cm^{-1}$ peak of $Cu(OH)_2$ as a function of time; laser power 90 mW: top- Compressed powder in 1M KOH; bottom- a metallic Cu surface with a $Cu(OH)_2$ surface film in 1M KOH.

5) Cyclic Voltrammogram of copper in 1M KOH at 10 mV/sec sweep rate. Major anodic and cathodic peaks identified. Potentials reported with respect to the Hg/HgO reference electrode in the same solution.

6) Raman spectra of Cu in 1M KOH during a 0.5 mV/sec potential-scan shown at selected potentials. Exposure time 100 seconds. a) Anodic sweep. b) Cathodic sweep. Spectra are offset to improve readability.

7) Raman spectra of Cu in 1M KOH during 0.5 mV/sec potential-scan. Comparison of spectra taken at 450 and 650 mV.

8) Raman spectra of Cu in 6M KOH during a 1 mV/sec potential-scan. 1) Anodic Sweep, -50 to 550 mV, 2) Cathodic Sweep, 350 to -450 mV, 3) Cathodic Sweep, -450 to -850 mV. Spectra are offset to improve readability.

9) a) Cyclic voltammogram of copper in 1M KOH during a 1 mV/sec potential-scan b) Integrated Raman peak intensities vs. potential corresponding to voltammetry shown in a). Solid squares-anodic sweep, $Cu_2O$ 633 $cm^{-1}$ peak; solid circles-anodic sweep, $Cu(OH)_2$ 488 $cm^{-1}$ peak. Open squares-cathodic sweep, $Cu_2O$ peak; open circles- cathodic sweep, $Cu(OH)_2$ peak. Cathodic sweep intensities shown as negative values to improve readability.

10) a) Cyclic voltammogram of Cu in 6M KOH at 1 mV/sec. b) Integrated Raman peak intensities corresponding to voltammetry in a). Solid squares- anodic sweep $Cu_2O$ 633 $cm^{-1}$ peak; solid circles-anodic sweep $Cu(OH)_2$ 488 $cm^{-1}$ peak; open squares-cathodic sweep $Cu_2O$ peak; open circles- cathodic sweep $Cu(OH)_2$ peak. Cathodic sweep intensities shown as negative values to improve readability.

11) Scanning electron micrograph of a copper surface oxidized in 1M KOH by a 0.5 mV/sec potential sweep. Maximum potential 100 mV vs. Hg/HgO. Bar at bottom is equal to 6.45 μm and applies to the left half of the figure. Area inside white box in left half shown ten times magnified in right half of figure.

12) Integrated Raman peak intensities for $Cu_2O$ (solid squares) and $Cu(OH)_2$ (open squares)during application of a potential program shown by the straight line segments.

13) Current (dotted line), potential (dashed line) and Raman peak intensity for $Cu_2O$ (633 $cm^{-1}$ solid line and squares) versus time in 1M KOH. Area of laser illumination changed during the potentiostatic portion of the experiments (at 1200 seconds). (a) at 500 mV, (b)

at 600 mV. Increase and decay of Raman signal in (a) shows presence of $Cu_2O$ not reduced at that potential in the dark.

14) a) Current response after a potential-step change from -600 to -150 mV in 1M KOH. b) Corresponding Raman spectra at different times.

15) Integrated Raman peak intensities for experiment shown in Figure 14. a) $Cu(OH)_2$ peak. b) $Cu_2O$ peak.

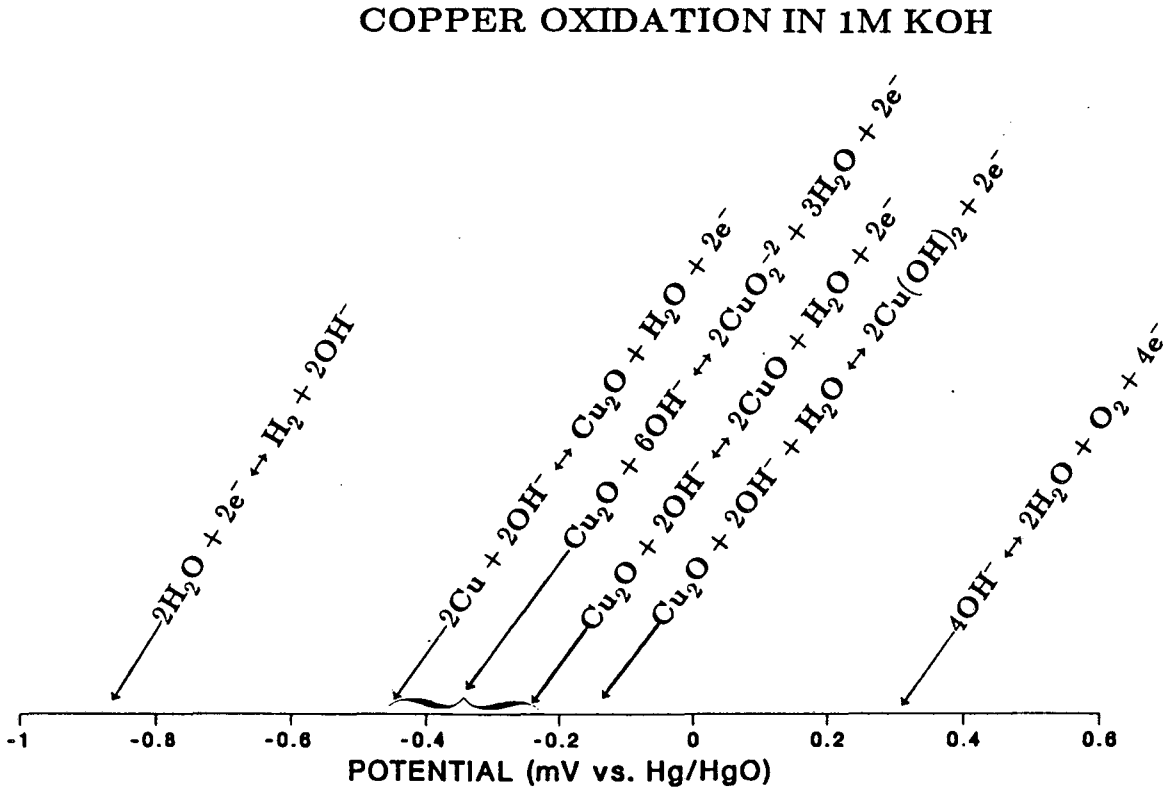


XBL 897-2624

Figure 1

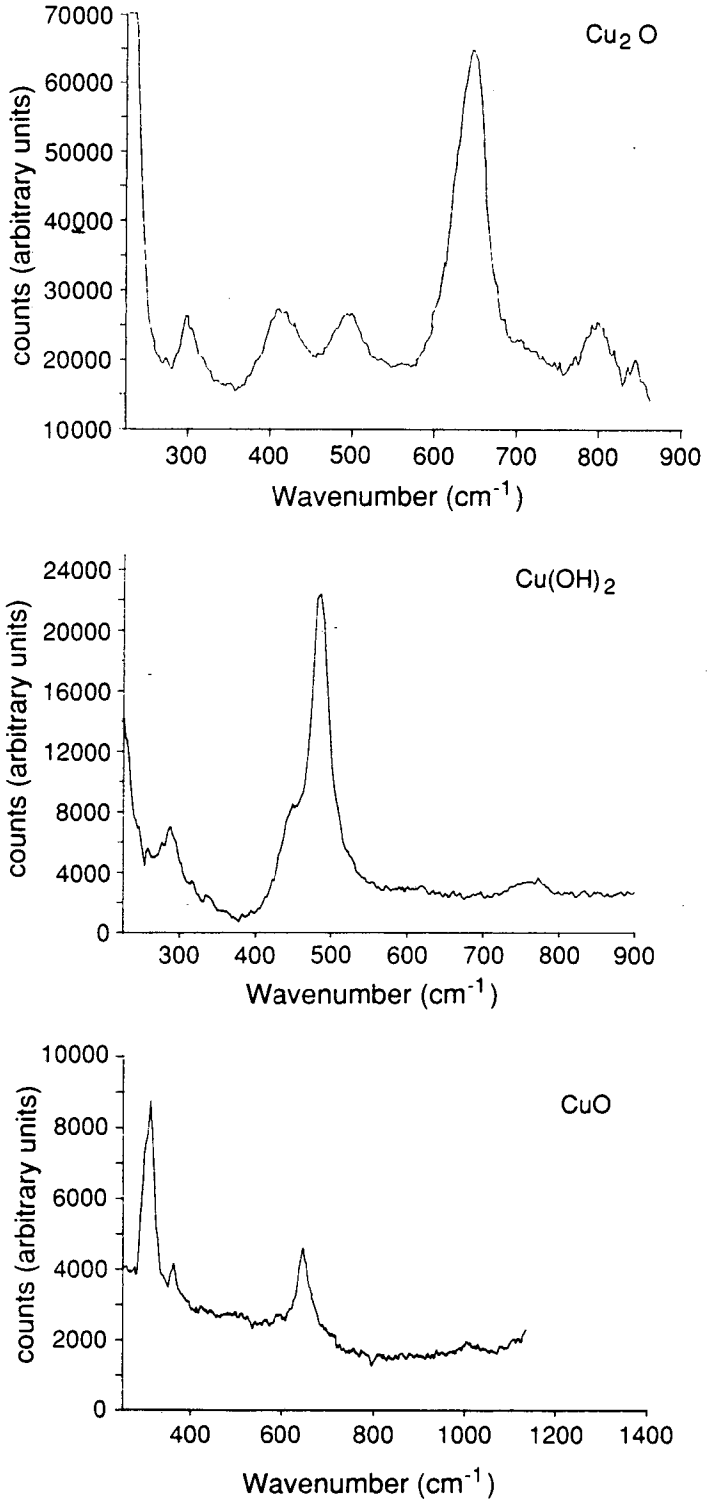


XBL 911-6007

Figure 2

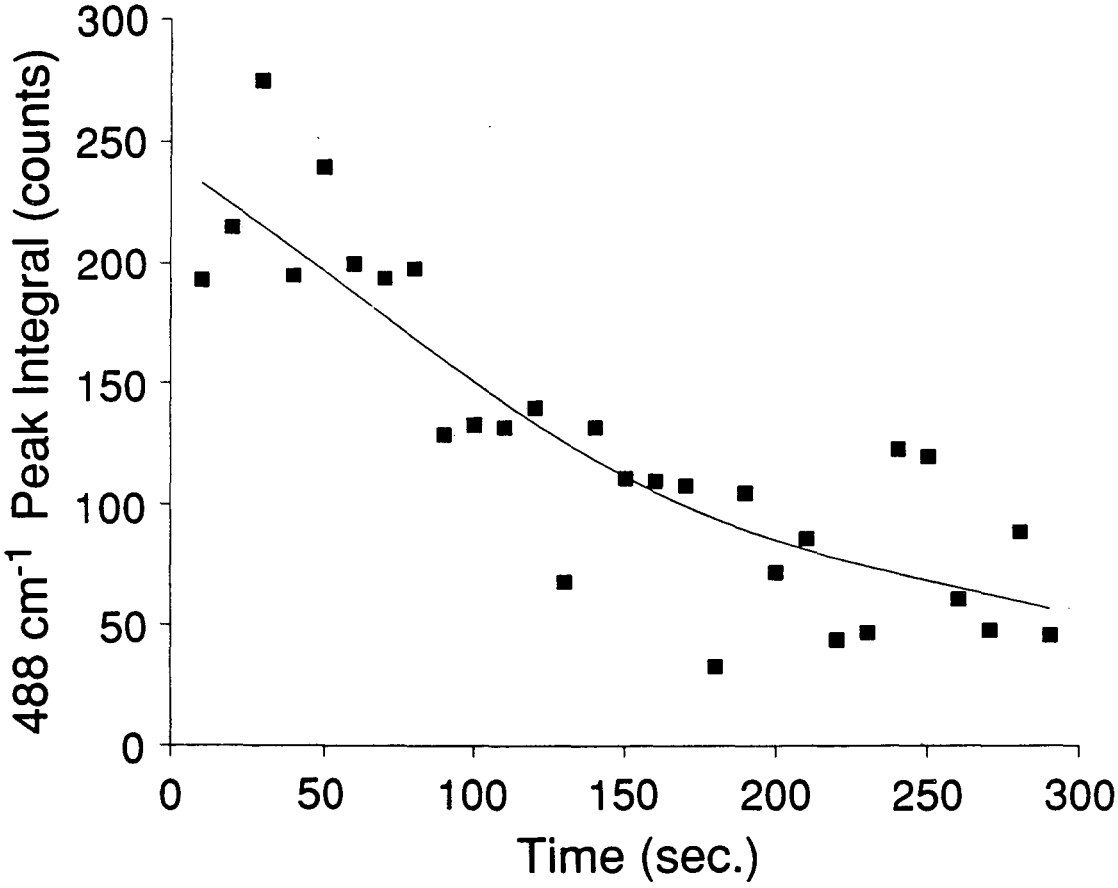


XBL 911-6006

Figure 3

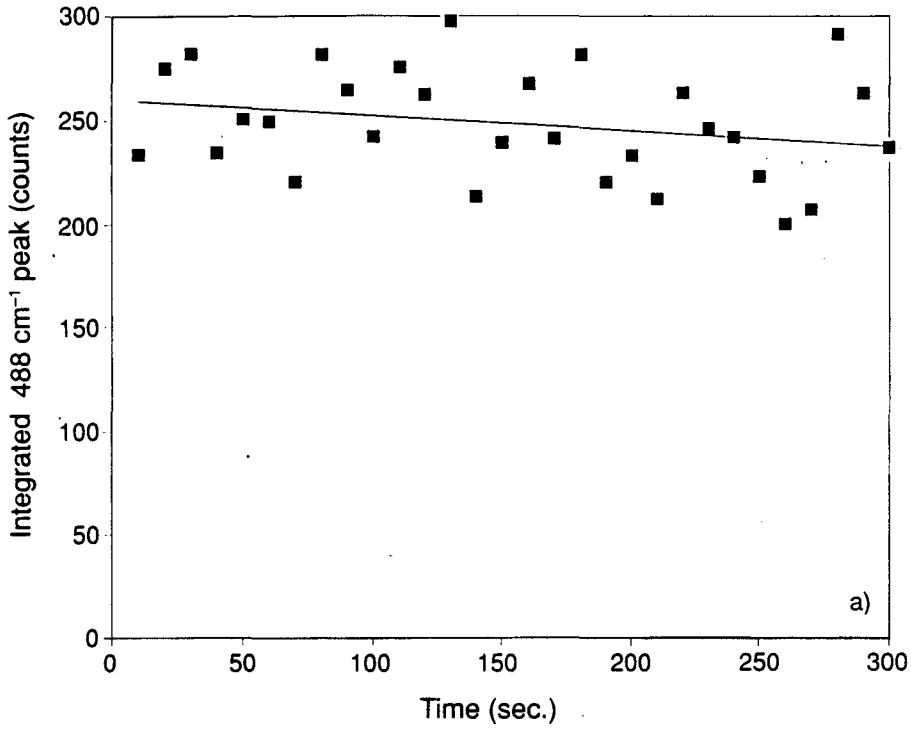


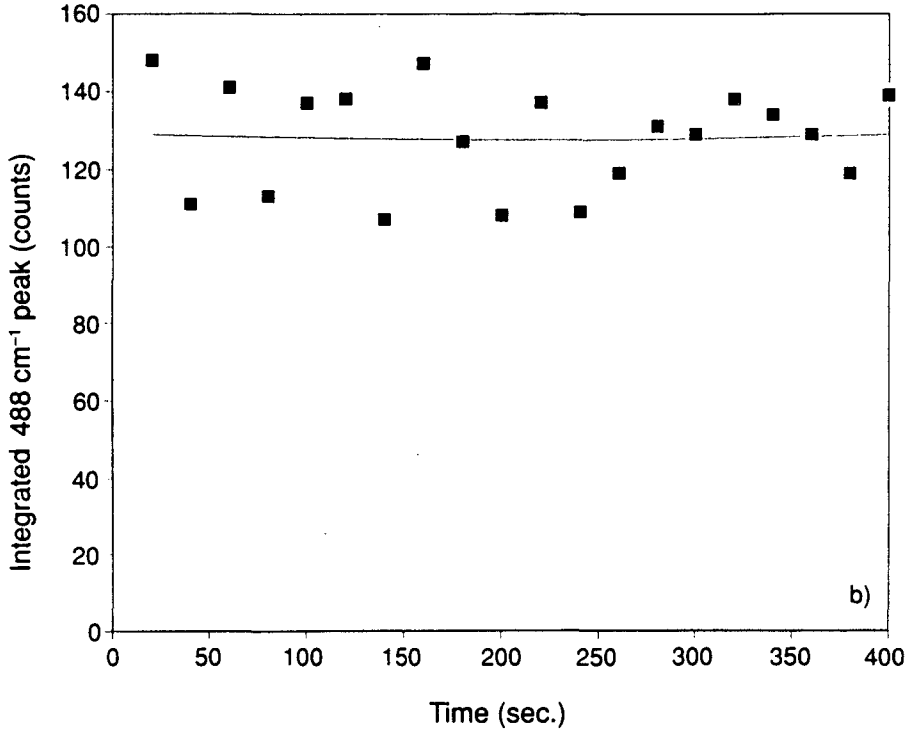


XBL 899-7293

Figure 4

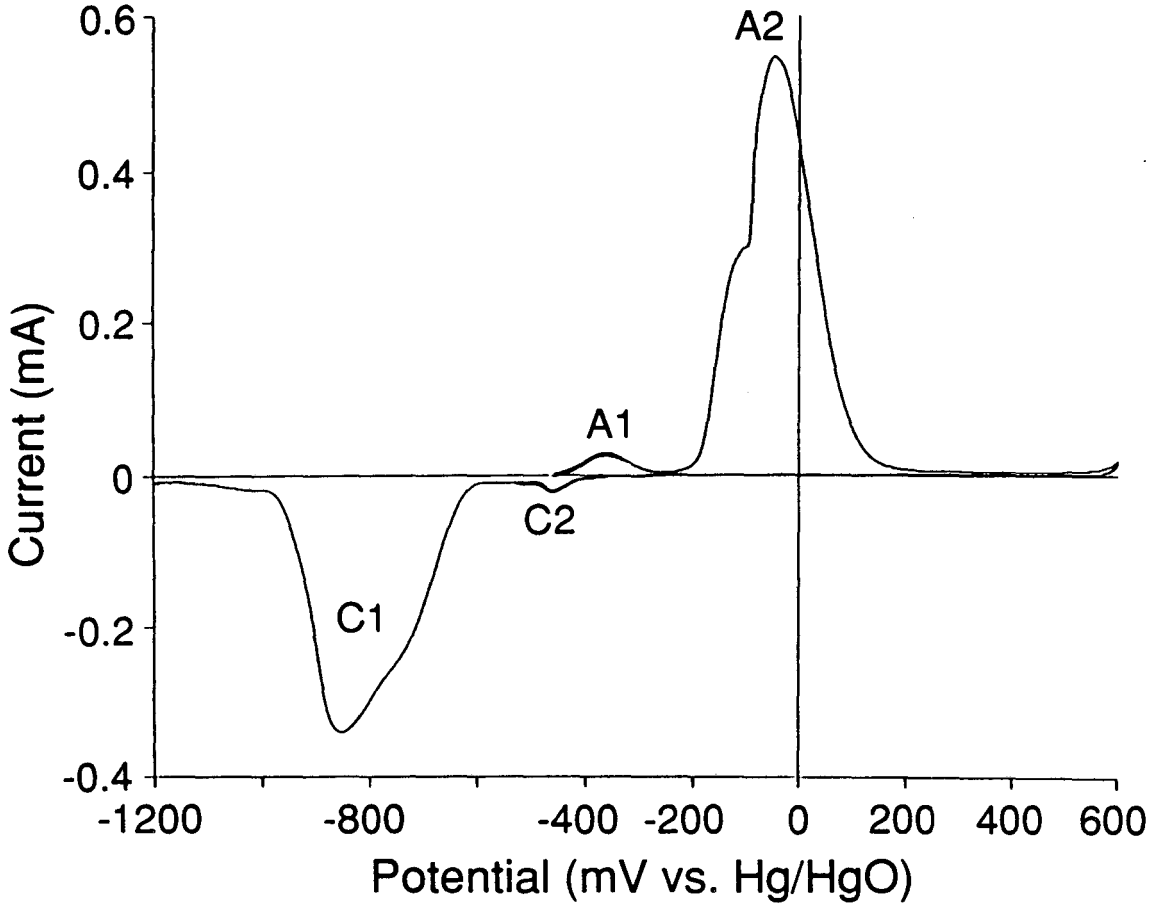


XBL 911-6005

Figure 5

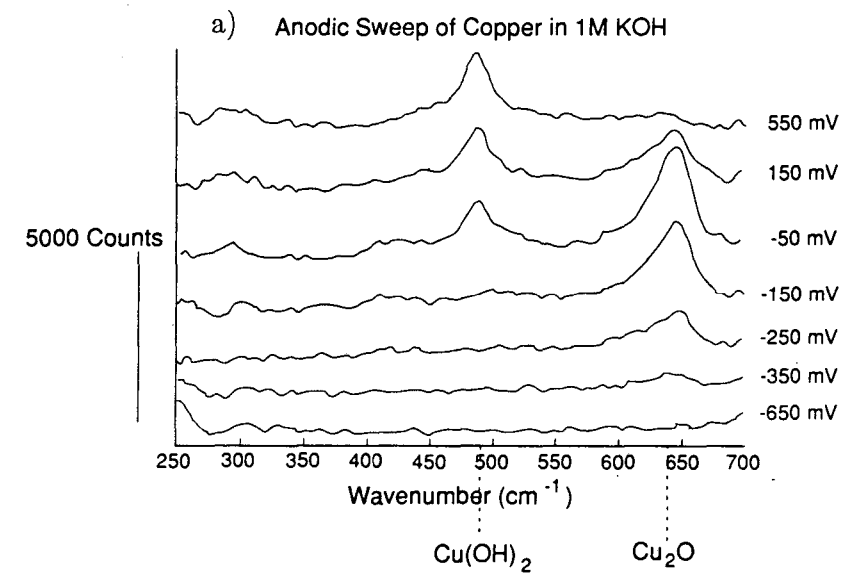


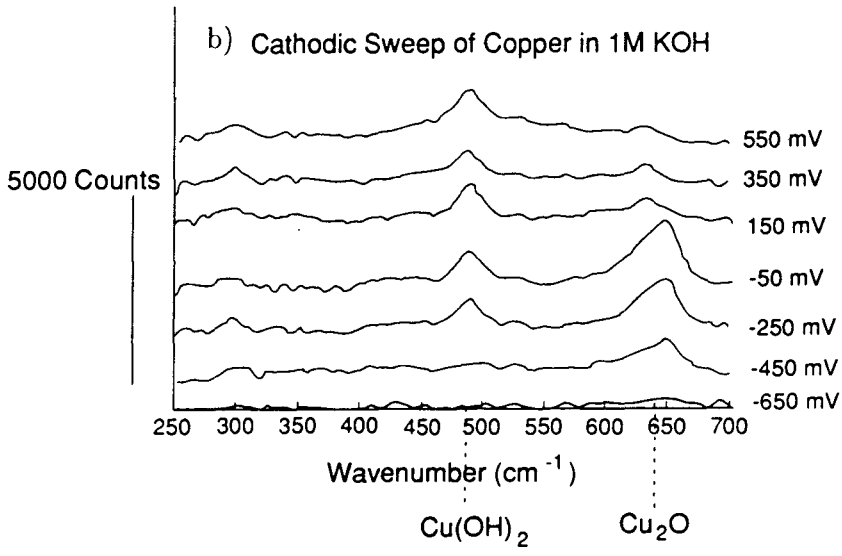


XBL 891-348A

Figure 6

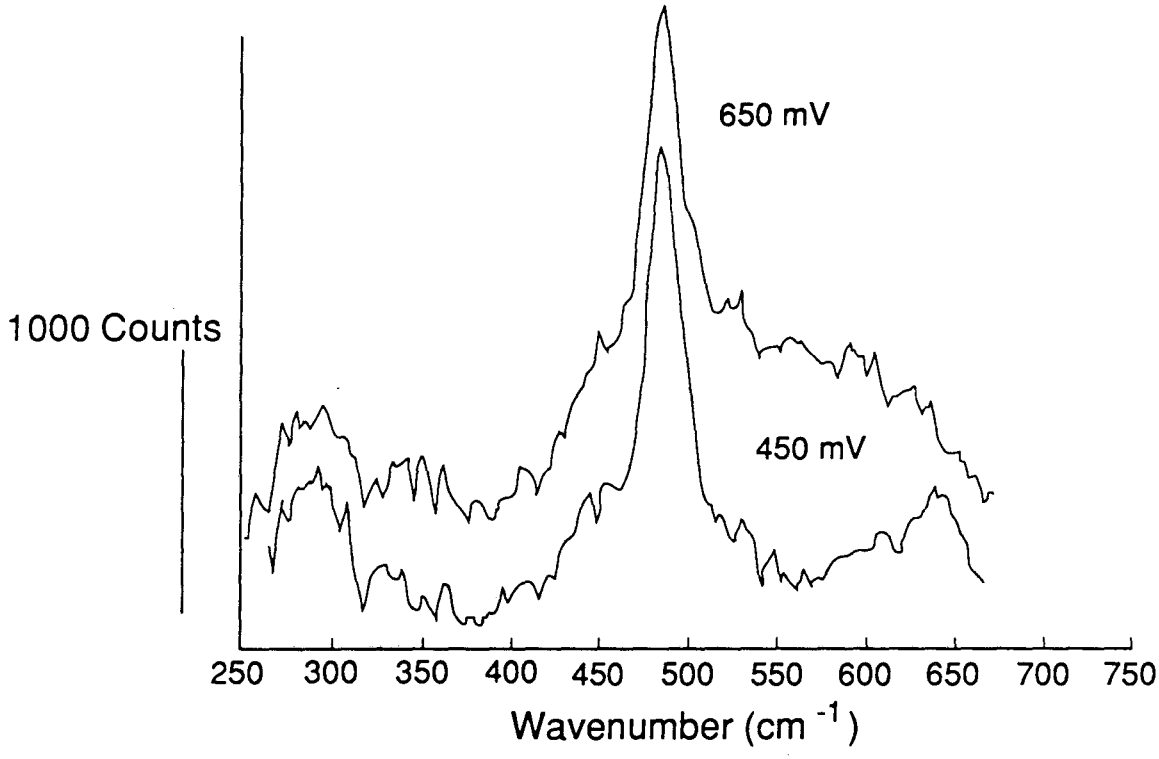


XBL 891-347

Figure 7

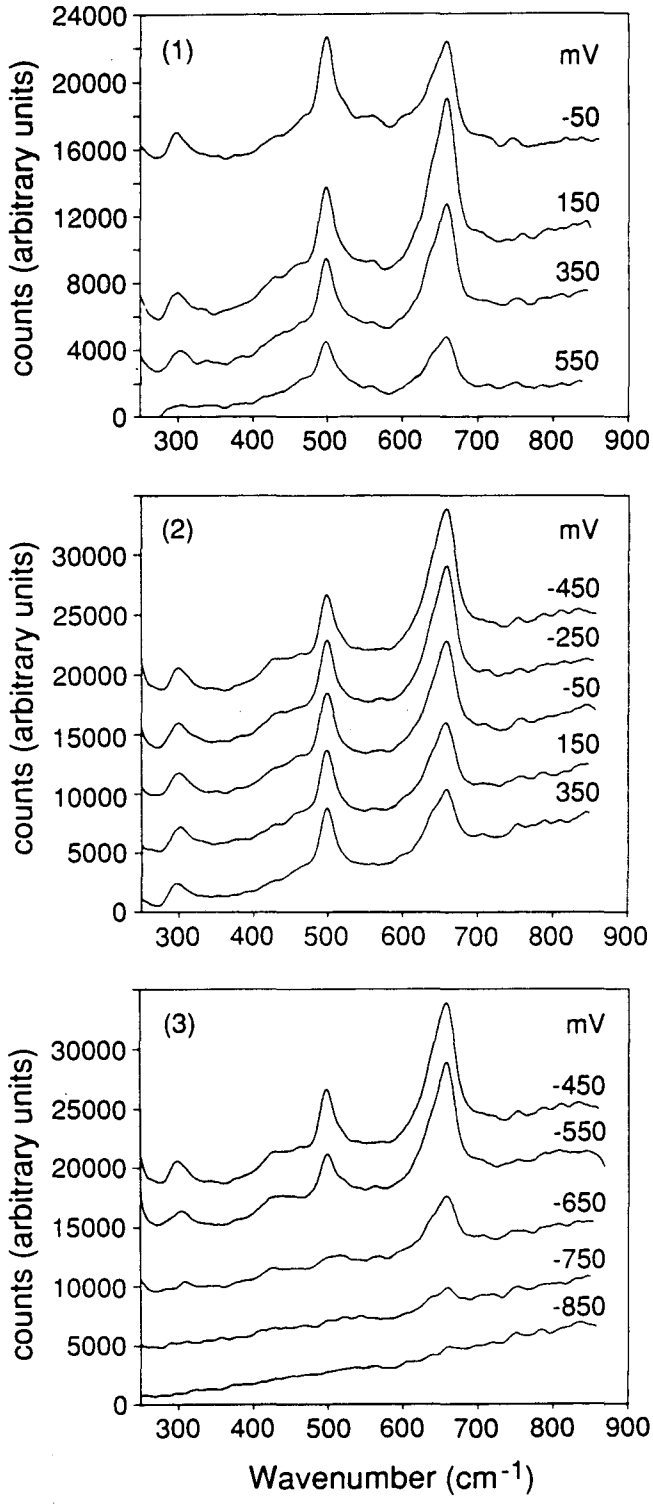


XBL 911-6004

Figure 8

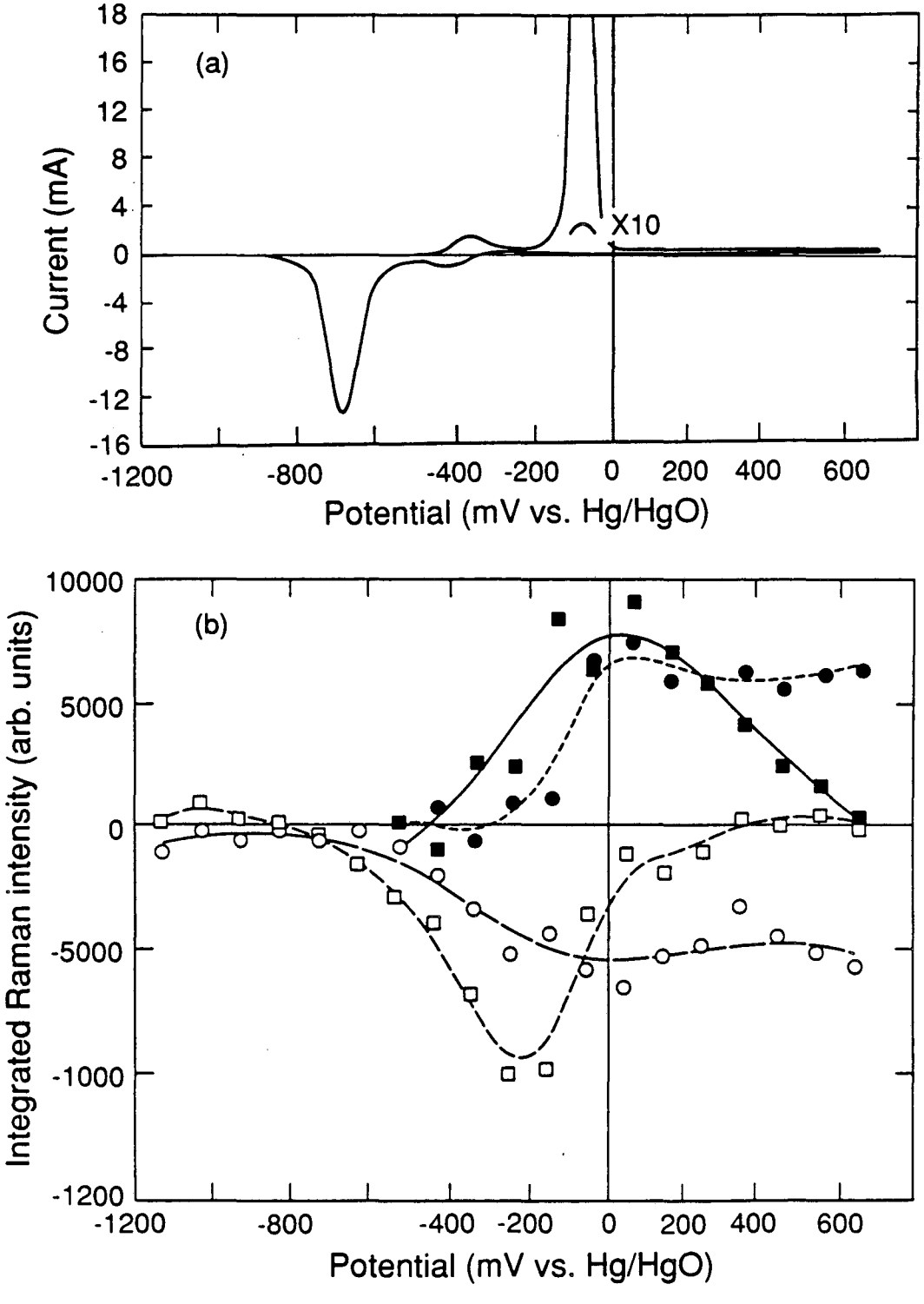


XBL 911-6003

Figure 9

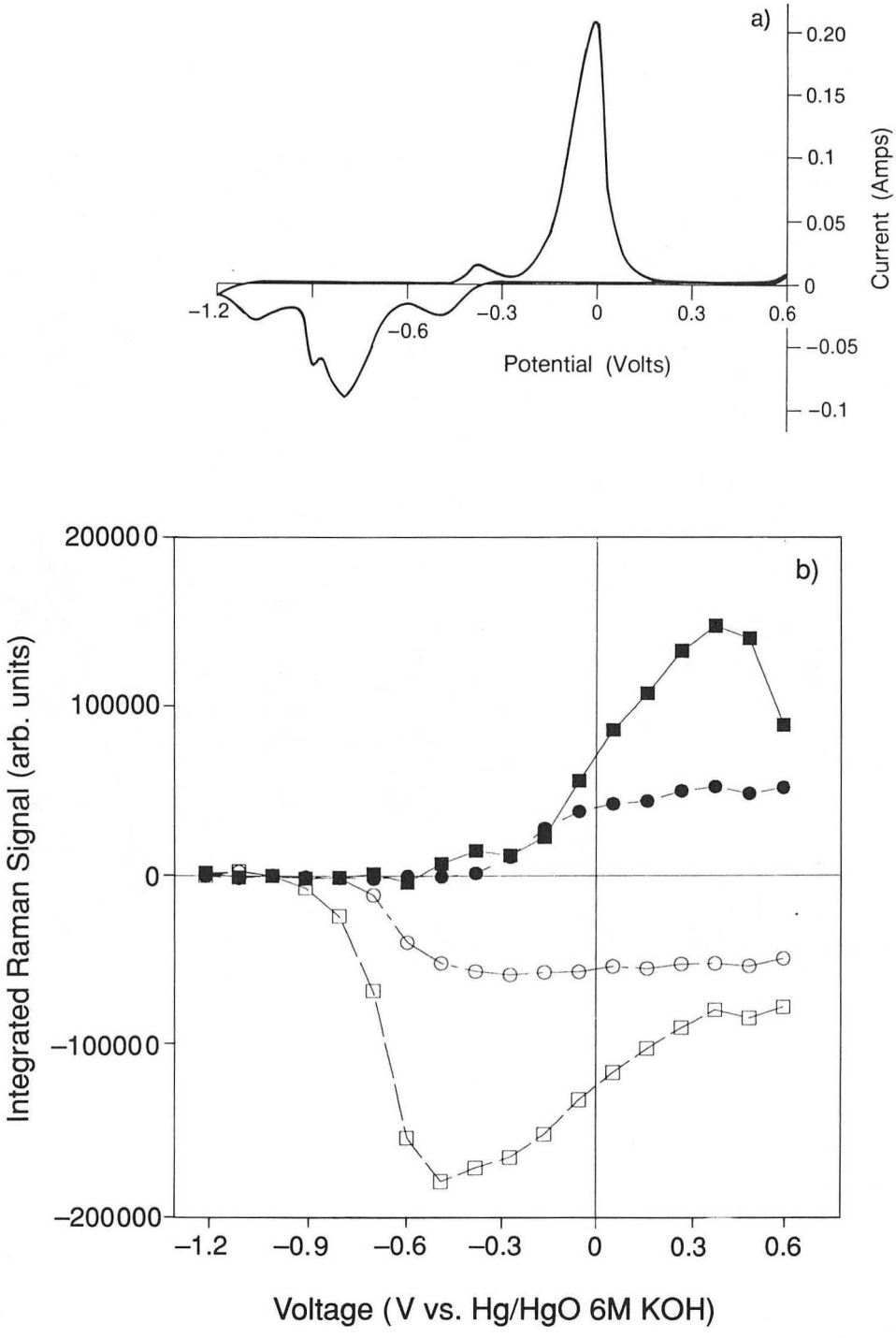


XBL 899-7299

Figure 10

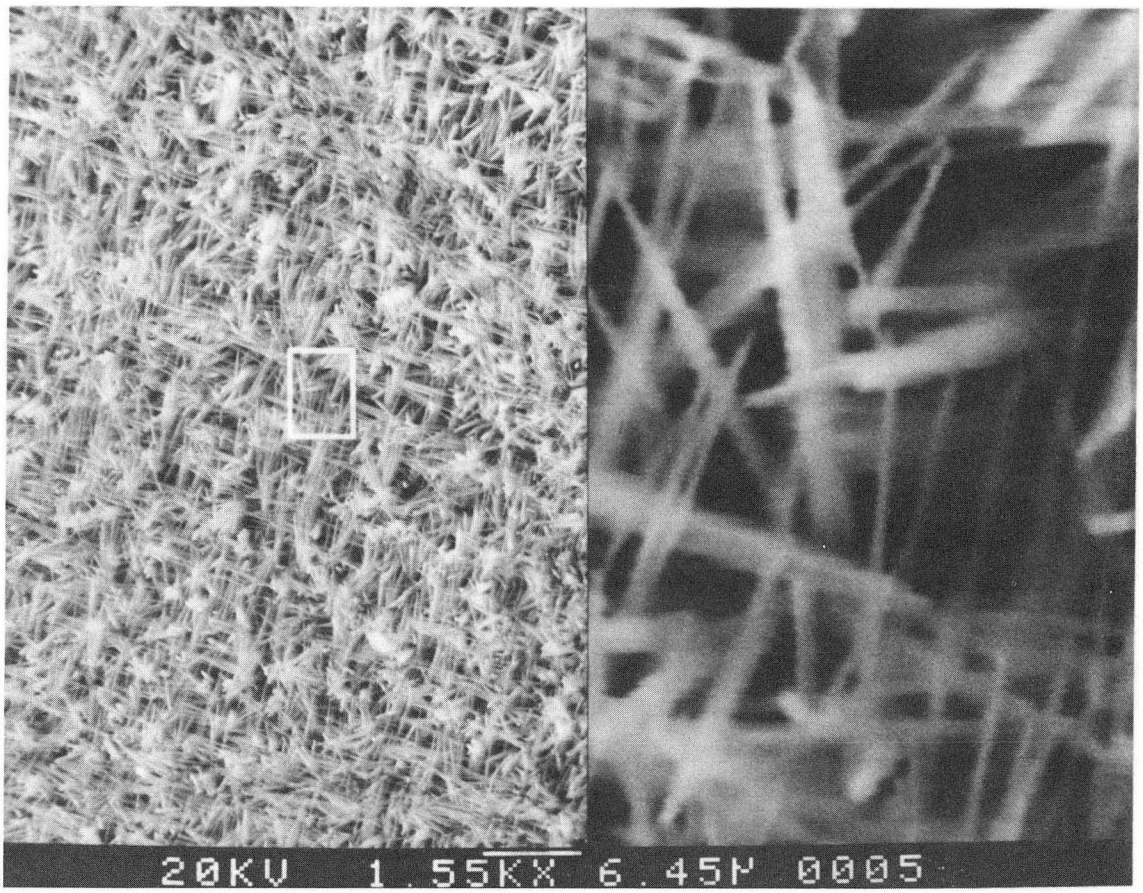


Figure 11

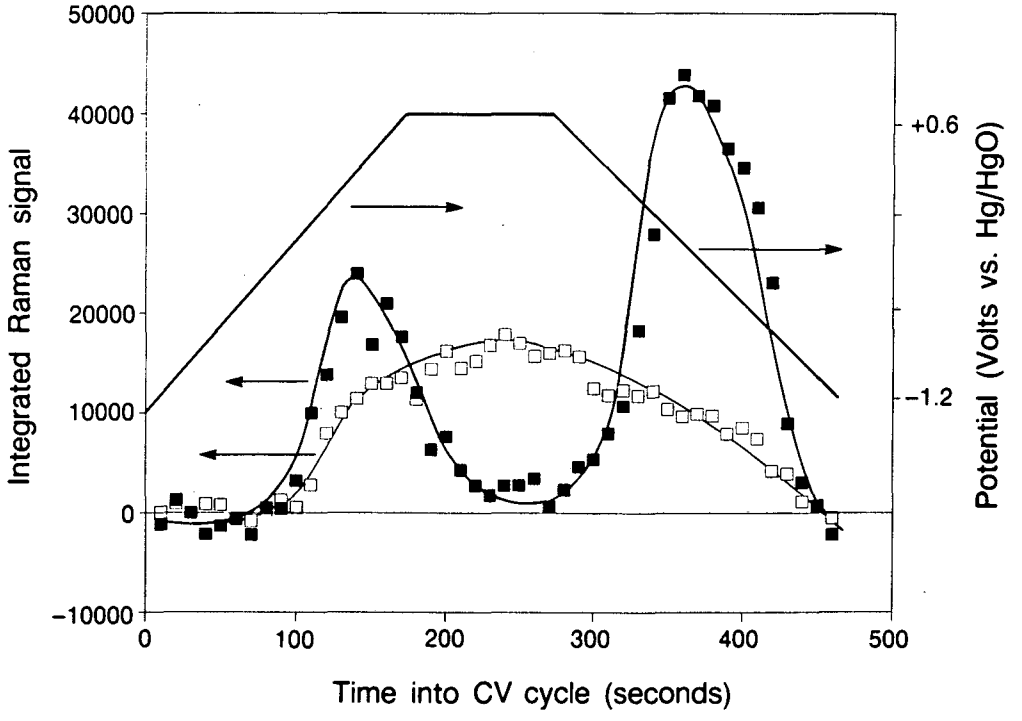


XBL 898-7252

Figure 12

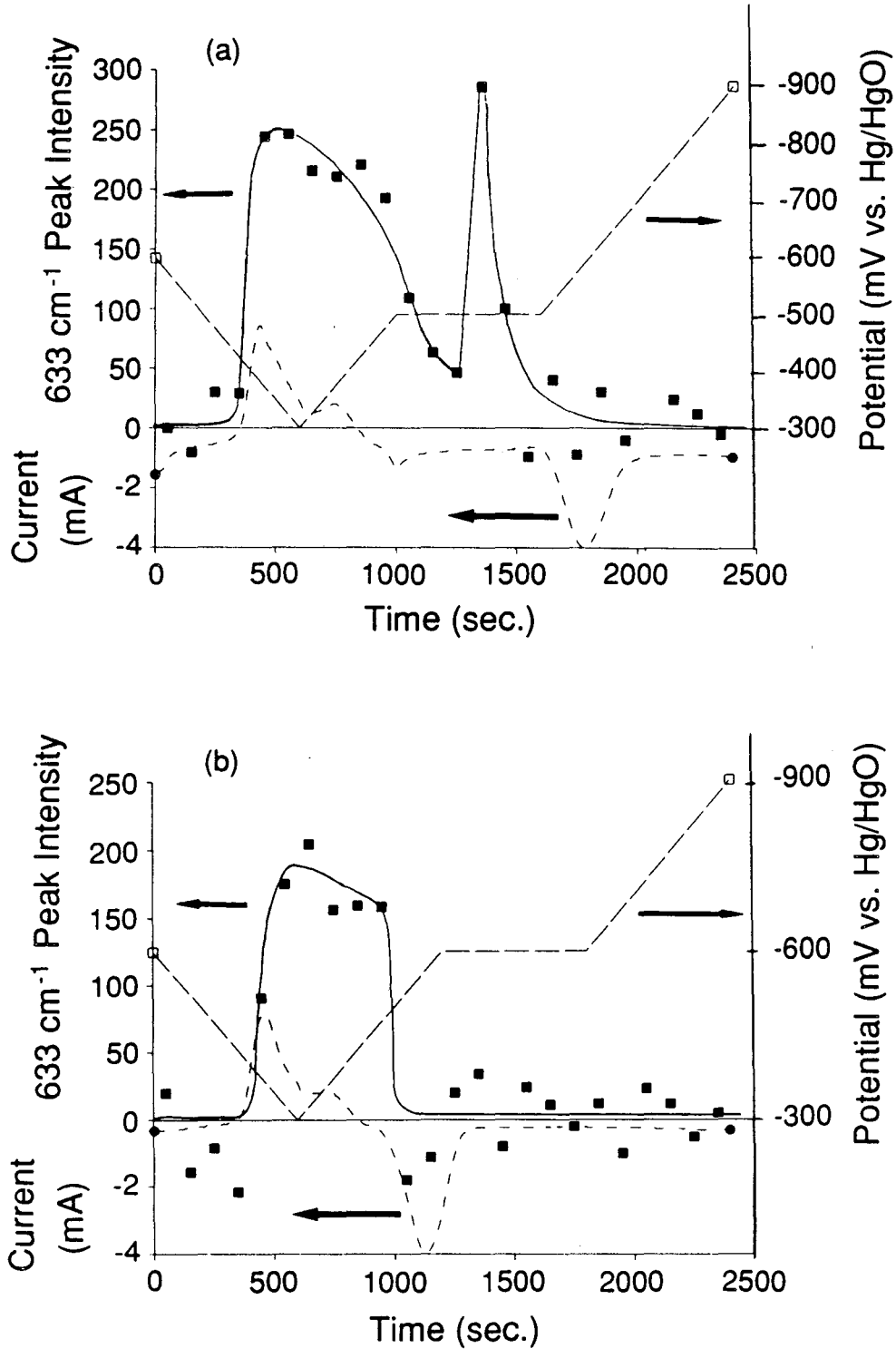


XBL 911-6002

Figure 13

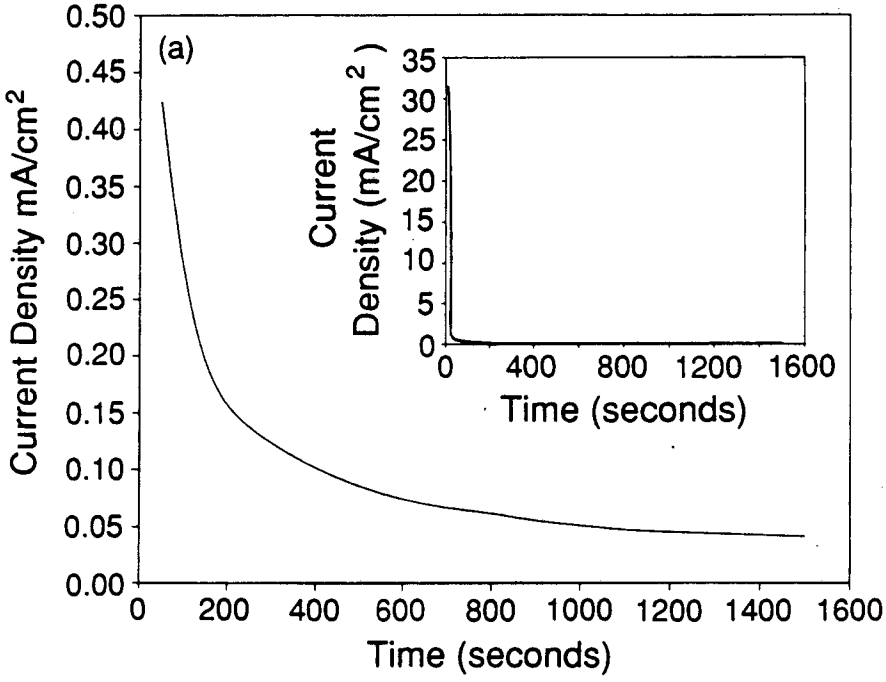


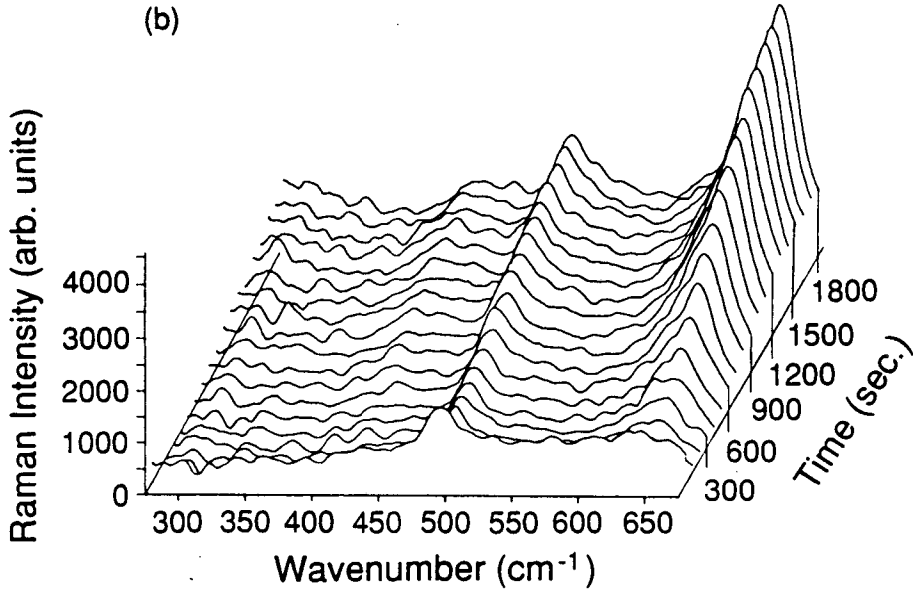


XBL 911-6001

Figure 14

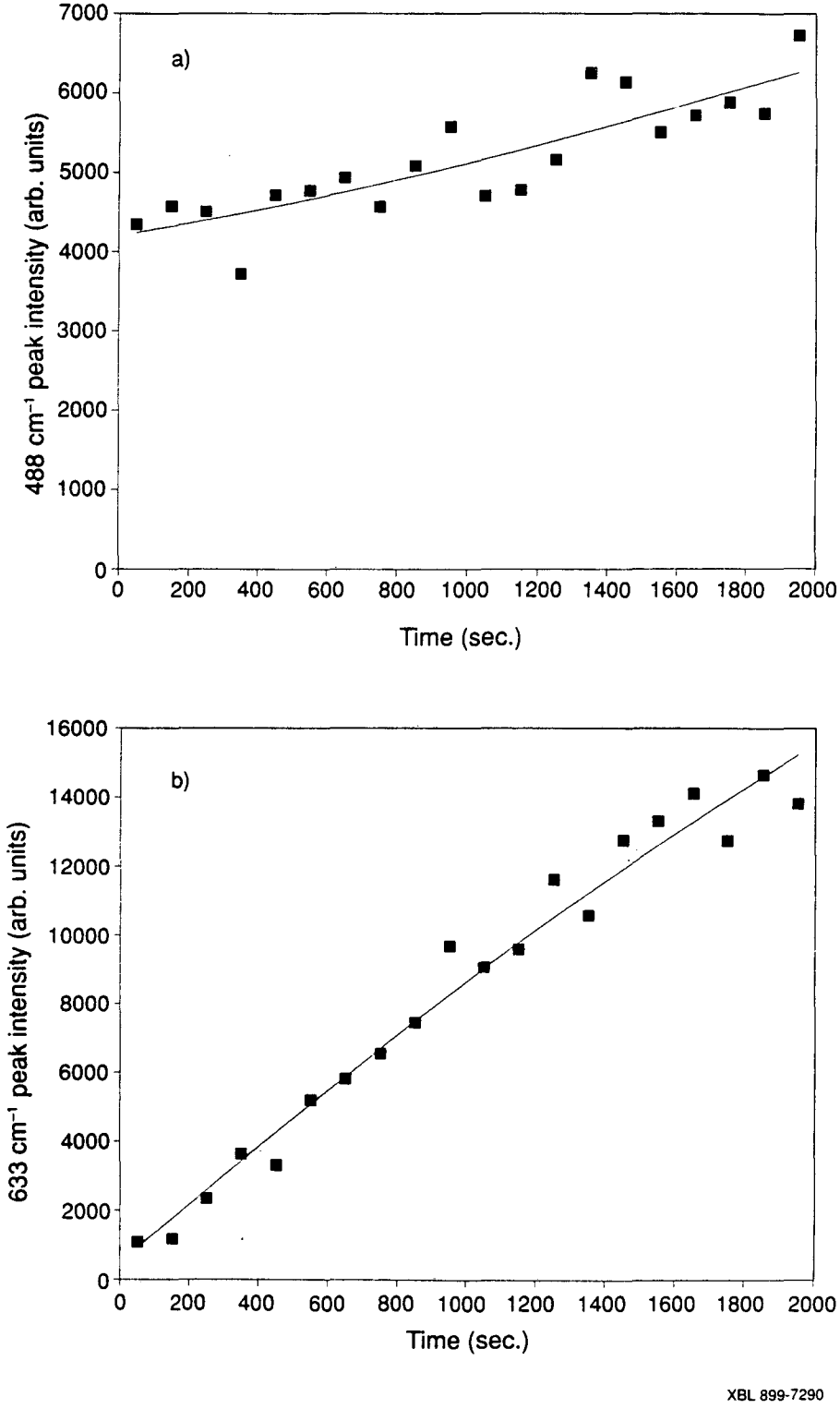
a)
488 cm⁻¹ peak intensity (arb. units)
0
1000
2000
3000
4000
5000
6000
7000
0
200
400
600
800
1000
1200
1400
1600
1800
2000
Time (sec.)
b)
633 cm⁻¹ peak intensity (arb. units)
0
2000
4000
6000
8000
10000
12000
14000
16000
0
200
400
600
800
1000
1200
1400
1600
1800
2000
Time (sec.)
XBL 899-7290

Figure 15

LAWRENCE BERKELEY LABORATORY
UNIVERSITY OF CALIFORNIA
INFORMATION RESOURCES DEPARTMENT
BERKELEY, CALIFORNIA 94720